Article type: Research Article

Title: Multifunctional PVA/MXQD Hydrogels for Integrated Flexible Strain Sensing and Solid-State Energy Storage Systems

Emad S. Goda[a], Jae Sang Cho[b], Dong Hwan Wang[a,b]*

[a]School of Integrative Engineering, Chung-Ang University, 84 Heukseok-ro, Dongjak-gu, Seoul 06974, Republic of Korea.
[b]Department of Intelligent Semiconductor Engineering, Chung-Ang University, 84 Heukseok-ro, Dongjak-gu, Seoul 06974, Republic of Korea.
* Corresponding authors, E-mail address: king0401@cau.ac.kr (Prof. Dong Hwan Wang)

1. Characterization:

The surface morphologies, dimensions, and elemental compositions of the prepared samples were examined using field-emission scanning electron microscopy (FESEM, Hitachi SU8010) coupled with energy-dispersive X-ray spectroscopy (EDX). The chemical structures of dried samples were further analyzed using Fourier-transform infrared (FTIR) spectroscopy, Raman spectroscopy, and powder X-ray diffraction (XRD). FTIR spectra were recorded on a Thermo Scientific Nicolet iS5 spectrometer using OMNIC software over the range of 4000–400 cm^{-1} at ambient conditions. XRD patterns were collected using a Philips X'Pert Pro powder diffractometer.

2. Mechanical characterization

The tensile properties of all hydrogel samples were evaluated using an Instron 3342 universal testing machine. Hydrogel films were cut into rectangular specimens with a width of 3.5 mm and a total length of 10 mm, yielding an effective gauge length of 5 mm. Uniaxial tensile tests were performed at a constant crosshead speed of 50 mm min^{-1}.

3. Electrochemical characterization of gel-state PPy@MXene//PPy@MXene supercapacitors

Electrochemical measurements of the all-gel-state supercapacitor devices (1 cm × 1 cm × 0.2 cm) were conducted using an Ivium potentiostat in a two-electrode configuration. Prior to testing, the PVA/MXQD hydrogel electrolyte, sandwiched between the electrodes, was immersed in 1 M H_2SO_4 for 1 h to form a solid-state device. Carbon cloth strips were used as current collectors and connected to conductive leads on both sides of the device. The assembled supercapacitor was sealed with parafilm to prevent moisture loss during measurements.

Cyclic voltammetry (CV) was performed at scan rates of 5–50 mV s^{-1}, while galvanostatic charge–discharge (GCD) tests were conducted at current densities ranging from 1 to 16 A g^{-1}. Electrochemical impedance spectroscopy (EIS) measurements were carried out over a frequency range of 0.01 Hz to 100 kHz with a 5 mV perturbation at open-circuit potential. The device's flexibility was evaluated by recording CV curves under different bending angles.

4. Calculation methods

The specific capacitance (C) of the gel-state supercapacitor was calculated from the GCD curves using:

$$C = 2I\,t/(m\,V) \quad (1)$$

where I is the discharge current, t is the discharge time, m is the total mass of the electrodes (g), and V is the applied voltage window.

The energy density (E_d) and power density (P_d) were calculated using:

$$E_d = \frac{C_{cell} * \triangle V^2}{2 * 3.6} \quad (2),$$

$$P_d = \frac{E_d * 3600}{t_d} \quad (3),$$

where C_{cell} is the cell capacitance and t_d is the discharge time [1, 2].

For human activity monitoring, the PVA/MXQD–CuNW sensor was attached to the body, and real-time current responses were recorded under various motions. Electrical current was

measured at a constant applied voltage of 2.0 V using a Keithley source meter. The relative change in resistance and gauge factor (GF) were calculated using:

$$\Delta R/R_0 = \frac{(R - R_0)}{R_0} \tag{4}$$

$$GF = \frac{\Delta R/R_0}{R_0} \tag{5}$$

where R_0 is the initial resistance, R is the real-time resistance during strain application, and ε is the applied strain on the hydrogel sensor.

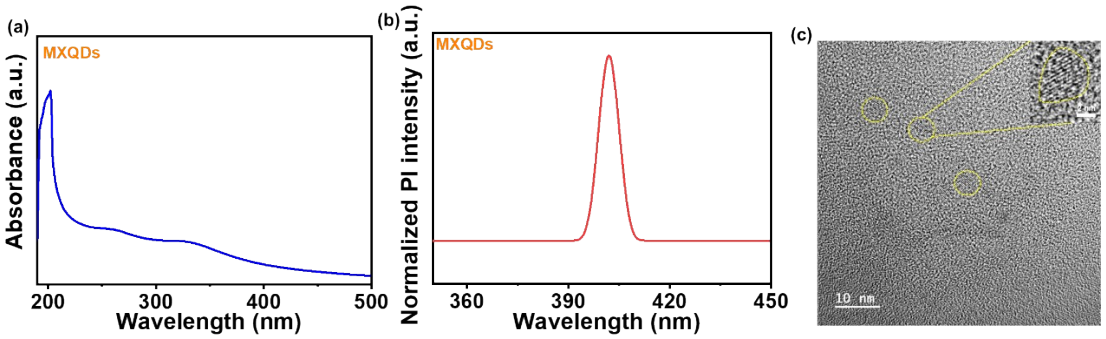

Fig. S1. (a) Absorption spectra and (b) Normalized PL spectra, and (c) TEM images for MXQDs.

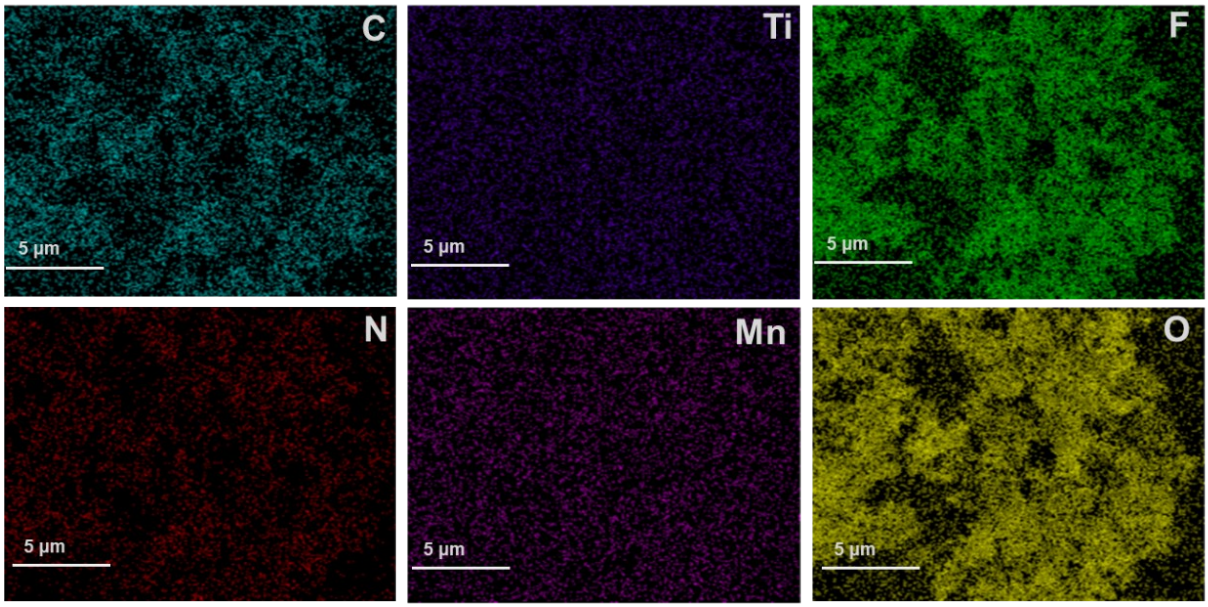

Fig. S2. EDS elemental mapping of the as-synthesized MXene@PPy composite.

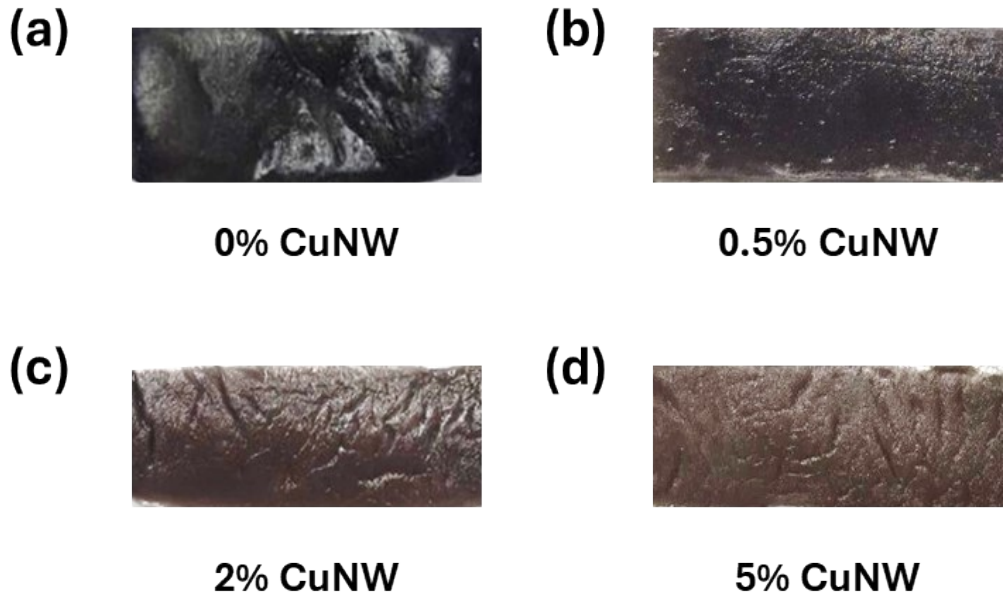

Fig. S3. Photographs of PVA/MXQD hydrogels containing 0%, 0.5%, 2%, and 5% (vol.%) CuNWs.

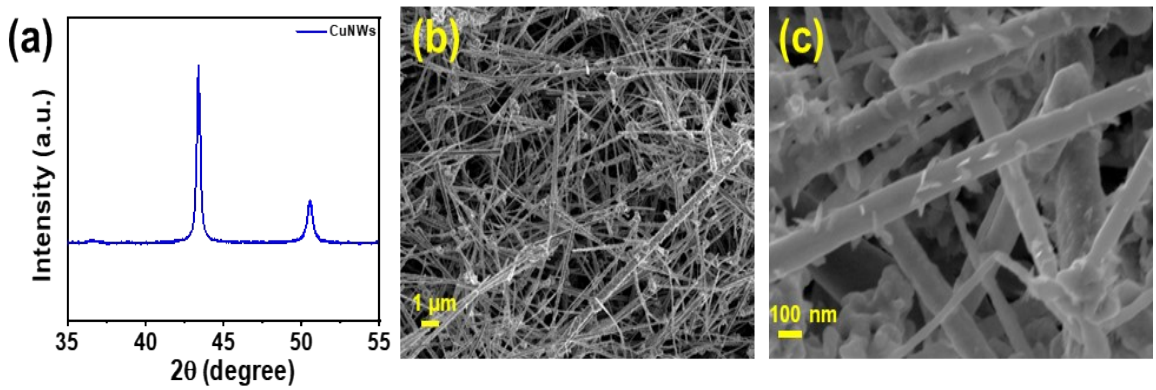

Fig. S4. (a) XRD pattern and (b, c) SEM images of CuNWs.

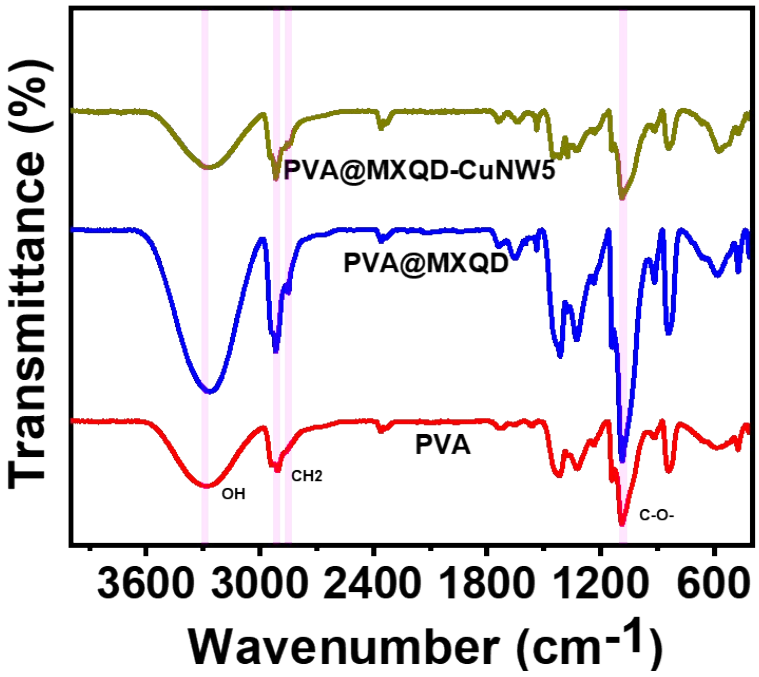

Fig. S5. FTIR spectra of PVA, PVA/MXQD, and PVA/MXQD–CuNW5.

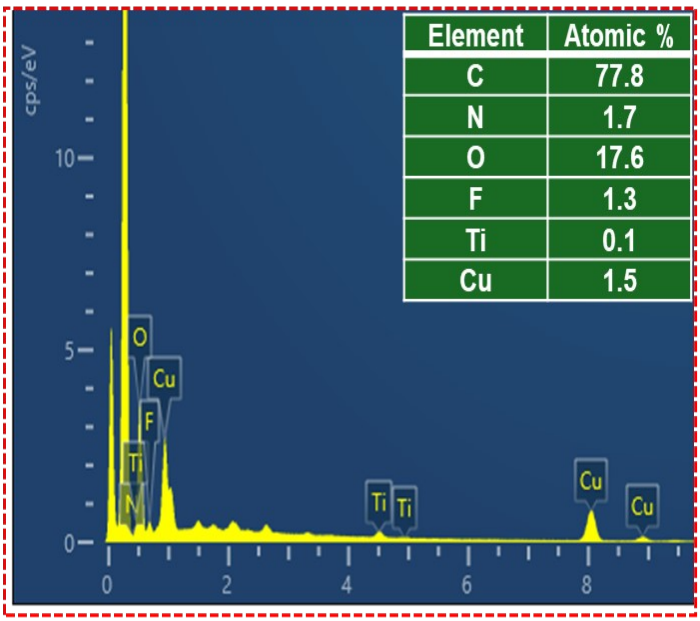

Fig. S6. EDS spectrum of PVA/MXQD–CuNW2 and corresponding elemental composition.

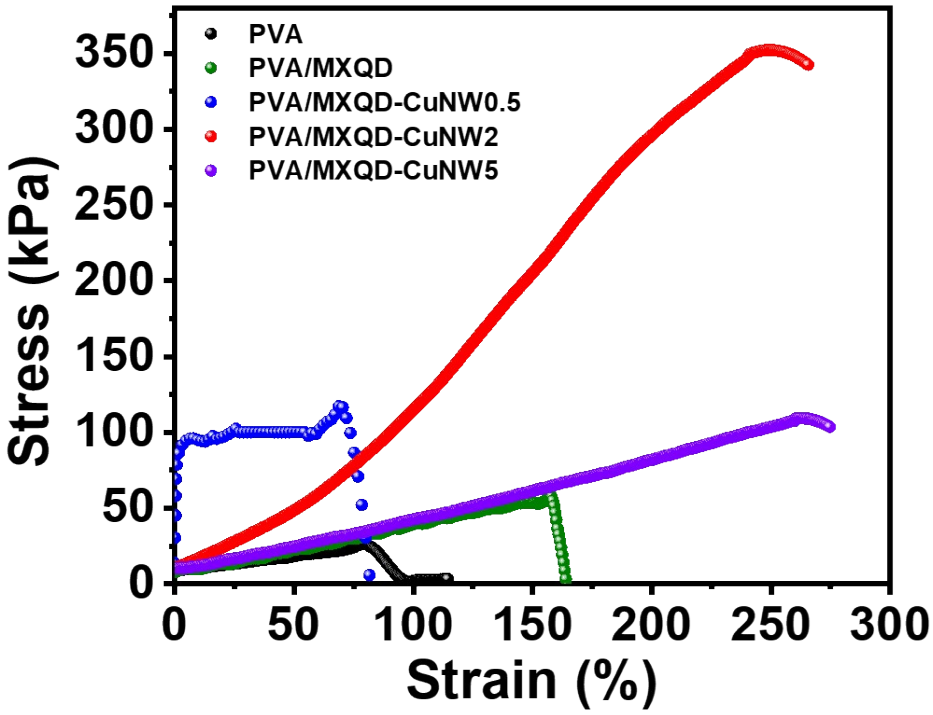

Fig. S7. Stress–strain curves for PVA, PVA/MXQD, PVA/MXQD–CuNW0.5, PVA/MXQD–CuNW2, and PVA/MXQD–CuNW5.

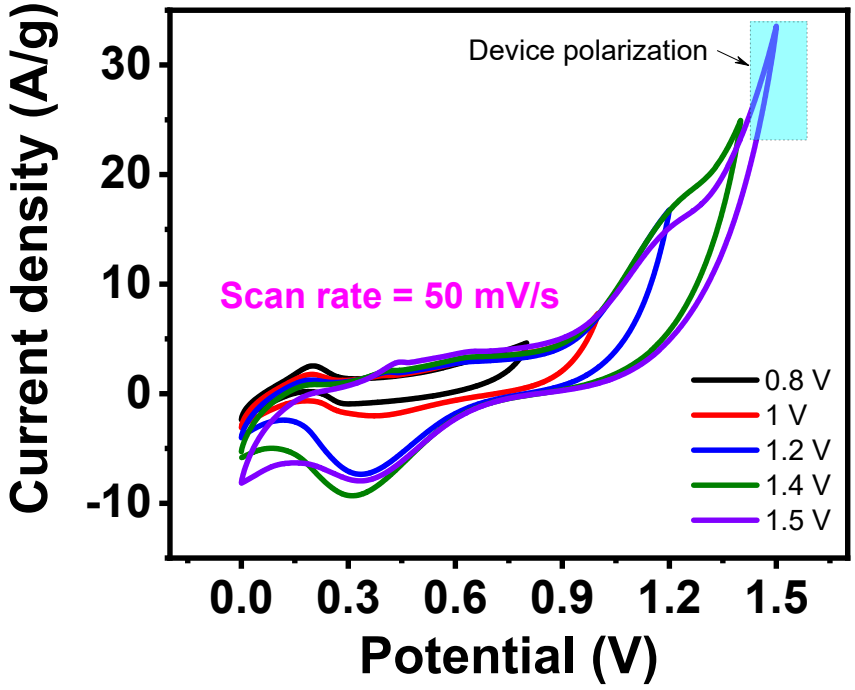

Fig. S8. CV curves of the symmetrical supercapacitor at various operating voltage ranges.

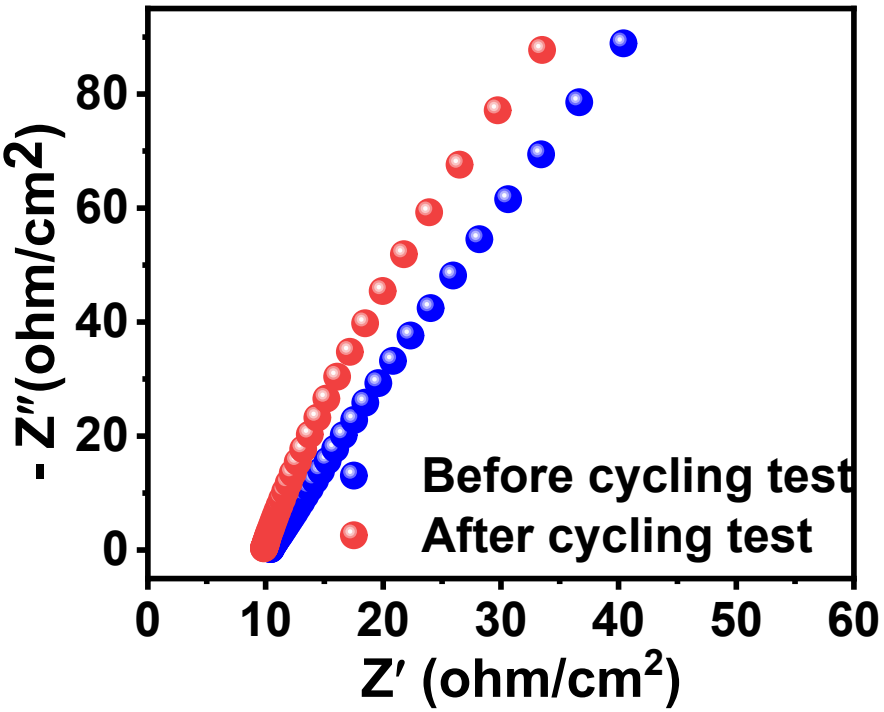

Fig. S9. Nyquist plots of the first and last cycles after 5000 cycling tests.

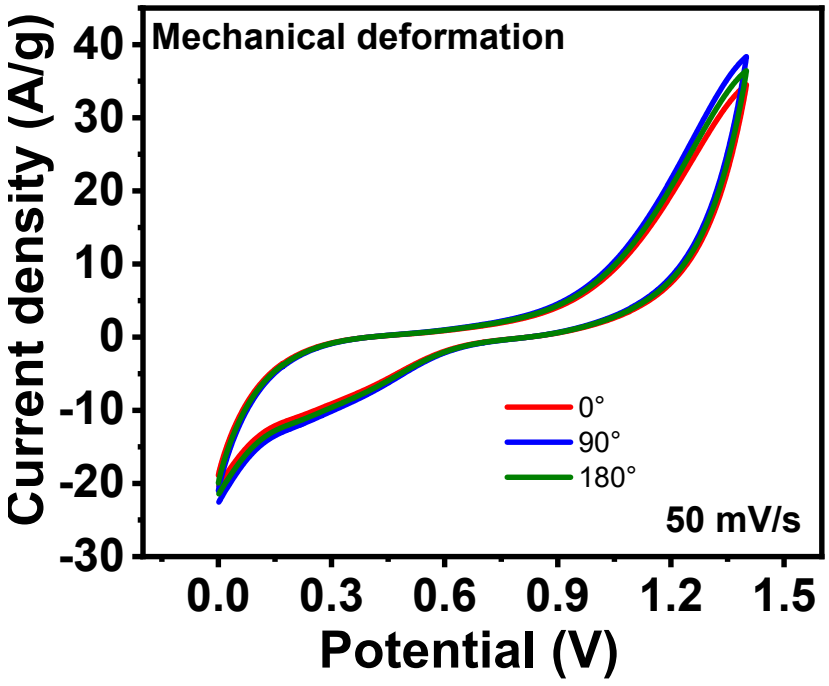

Fig. S10. CV curves of the symmetrical device under various bending angles.

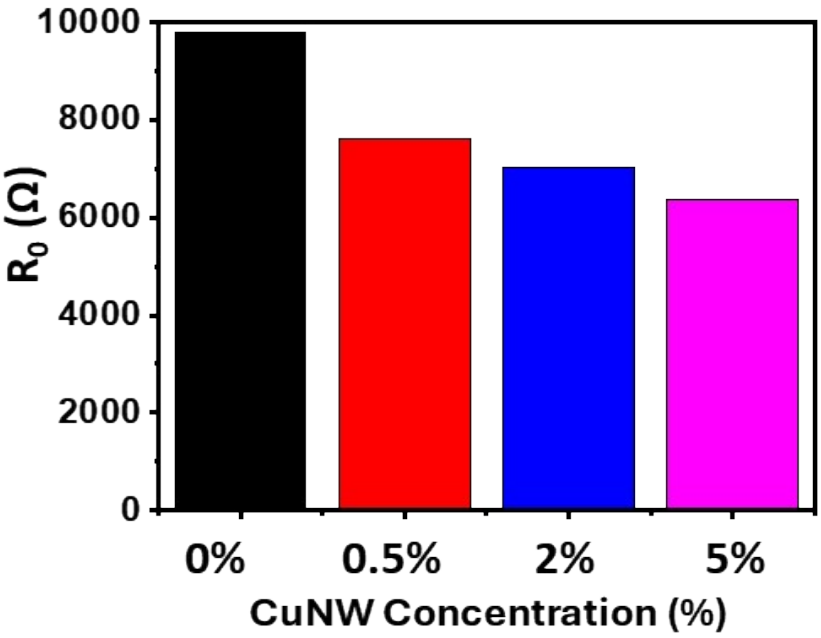

Fig. S11. Initial resistance (R_0) measured from the pristine hydrogels before application of strain as a function of CuNW content.

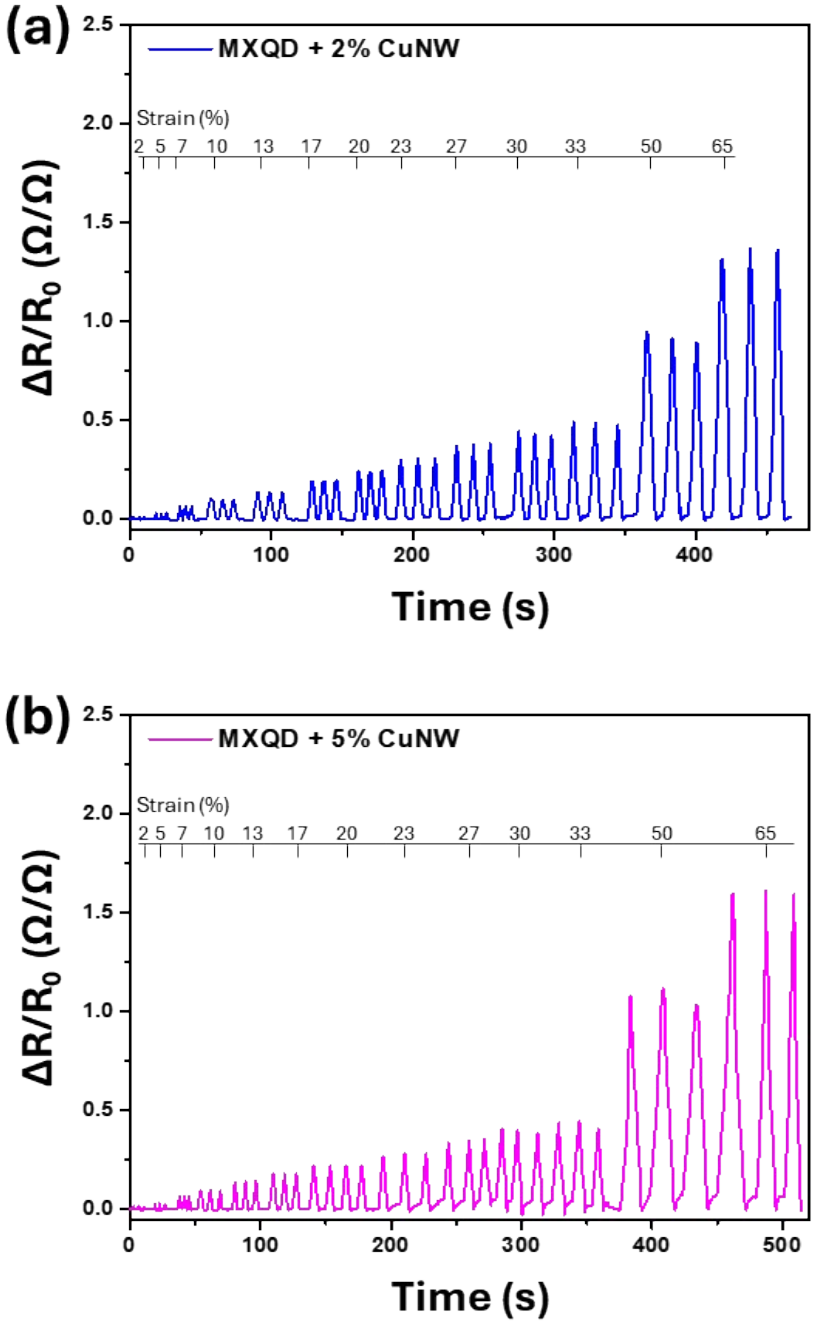

Fig. S12. Strain sensing results from PVA/MXQD–CuNW2 and PVA/MXQD–CuNW5.

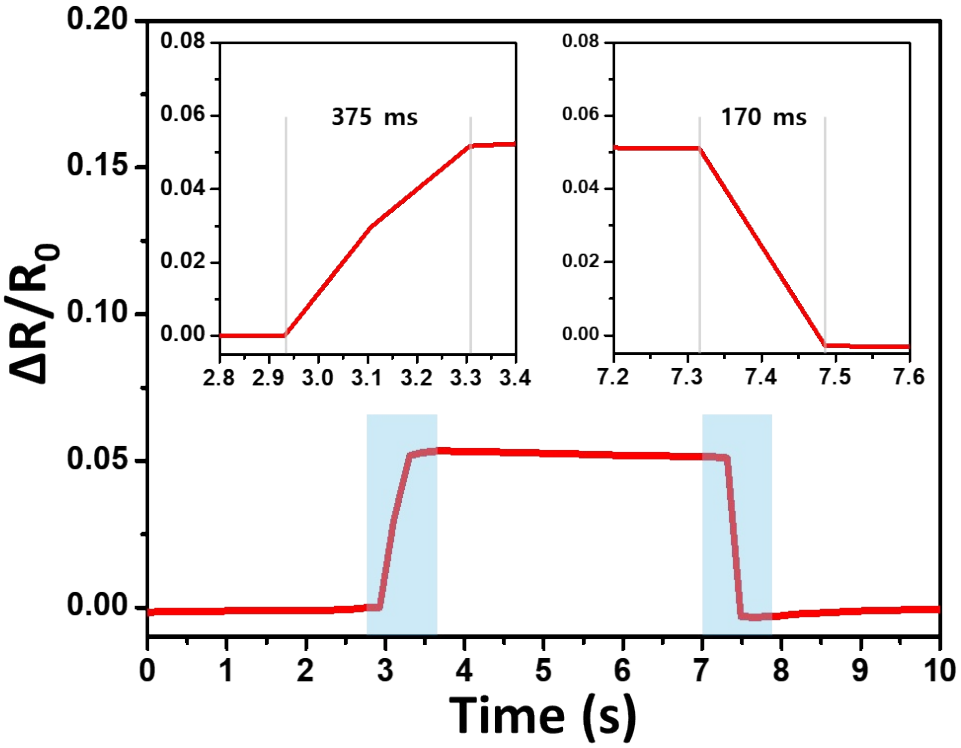

Fig. S13. Response time and recovery time of PVA/MXQD–CuNW hydrogel-based strain sensor.

Table S1. Comparison of our work with other reported flexible all-solid-state supercapacitors.

Electrolyte	Electrode	Device capacitance [F/g]	Energy density [Wh/kg]	Power density [kW/kg]	Capacitance retention	Ref.
PVA-PAM-ethylene glycol	PANI/ carbon cloth	185.1 (0.5 A/g)	16.1	1.43	86.5% (4000 C)	[3]
PVA-KC	AC	117.5 (0.5 A/g)	-	-	95% (2000 C)	[4]
PVA-H_2SO_4	Ppy hydrogel	268 (1.6 A/g)	62 (μWh cm^{-2})	0.57 (mW cm^{-2})	84% (1000 C)	[5]
Lignin/KOH	lignin/PAN carbon nanofiber	129.23 (0.5 A/g)	4.49	2.63	95% (10000 C)	[6]
PVA-H_2SO_4	All-in-one PANi/PVA	488 mF cm^{-2} (0.2 mA cm^{-2})	42 (μWh cm^{-2})	0.160 (mW cm^{-2})	90% (7000 C)	[7]
PVA-H_2SO_4	PPy/CuTcPs	505 mF cm^{-2} (2.0 mA cm^{-2})	44.9 (μWh cm^{-2})	8 (mW cm^{-2})	97% (2000 C)	[8]
PVA-boronic	PANI/ carbon cloth	153 (0.25 A/g)	13.6	0.105	90% (1000 C)	[9]
PVA/PAMAA	MWCNT film	75.8 mF cm^{-2} (0.5 mA cm^{-2})	10.52 (μWh cm^{-2})	0.25 (mW cm^{-2})	90.2% (5000 C)	[10]
PVA/MXQD-H_2SO_4	Ppy@MXene	165 (1 A/g)	44.8	0.715	71.4% (5000 C)	This work

Table S2. Comparison of our work with recently reported PVA based strain sensors.

Polymer Matrix	Conductive Filler	Gauge Factor (GF)	Ref. (Year)
PVA, Borax, IL	PEDOT:PSS	1.00	Meng et al. (2025)[11]
PVA, PAA	Conductive ions (Fe3+)	1.98	Zhang et al. (2025)[12]
PVA, CMCS	Tannic Acid, NaCl	2.37	Zhang et al. (2022)[13]
PVA, PAM	Polyaniline (PANI)	2.73	Cai et al. (2025)[14]
PVA, Gelatin	MXene, Tannic Acid	3.15	Chen et al. (2025)[15]
PVA, Borax, DNA	MXene, AuNP	4.90	Ghazizadeh et al. (2025)[16]
PVA	MXQD, CuNWs	3.50	This Work (2026)

References

1. E. S. Goda, B. Pandit, S. E. Hong, B. S. Singu, S. K. Kim, E. B. Moustafa and K. R. Yoon, *Journal of Energy Chemistry*, 2022, **74**, 429–445.
2. E. S. Goda, A. ur Rehman, B. Pandit, A. Al-Shahat Eissa, S. Eun Hong and K. Ro Yoon, *Chemical Engineering Journal*, 2022, **428**, 132470.
3. Z. Liu, J. Zhang, J. Liu, Y. Long, L. Fang, Q. Wang and T. Liu, *Journal of Materials Chemistry A*, 2020, **8**, 6219–6228.
4. X. Hu, L. Fan, G. Qin, Z. Shen, J. Chen, M. Wang, J. Yang and Q. Chen, *Journal of Power Sources*, 2019, **414**, 201–209.
5. F. Chen, Q. Chen, Q. Song, H. Lu and M. Ma, *Advanced Materials Interfaces*, 2019, **6**, 1900133.
6. J. H. Park, H. H. Rana, J. Y. Lee and H. S. Park, *Journal of Materials Chemistry A*, 2019, **7**, 16962–16968.
7. K. Wang, X. Zhang, C. Li, X. Sun, Q. Meng, Y. Ma and Z. Wei, *Advanced Materials*, 2015, **27**, 7451–7457.
8. M. Guo, Y. Zhou, H. Sun, G. Zhang and Y. Wang, *Electrochimica Acta*, 2019, **298**, 918–923.
9. W. Li, F. Gao, X. Wang, N. Zhang and M. Ma, *Angewandte Chemie*, 2016, **128**, 9342–9347.
10. J. Huang, S. Peng, J. Gu, G. Chen, J. Gao, J. Zhang, L. Hou, X. Yang, X. Jiang and L. Guan, *Materials Horizons*, 2020, **7**, 2085–2096.
11. M. Meng, R. Fu, T. Xue, X. Liu, J. Jiang and X. Liu, *Chemical Engineering Journal*, 2025, **519**, 165709.
12. Y. Zhang, L. Liu, S. Yin, C. Zhou, Y. Ding, G. Che and C. Zhao, *Advanced Functional Materials*, 2025, **35**, 2503023.
13. L. Zhang, O. Hu, J. Zhang, L. Hou, D. Ye, X. Jiang and G. Xiao, *Cellulose*, 2022, **29**, 9323–9339.
14. J. Cai, S. Huang, W. Zhou, X. He, H. Liang, J. Zhou, C. Zhao and T. Xu, *Materials Today Communications*, 2025, **44**, 111976.
15. Y. Chen, W. Guo, N. Chen, Y. Liu, X. Wan, T. Wang, Z. Zhou, Y. Jin and G. Li, *Sensors and Actuators A: Physical*, 2025, **383**, 116231.
16. E. Ghazizadeh, H.-P. Deigner, M. Al-Bahrani, K. Muzammil, N. Daneshmand and Z. Naseri, *Sensors and Actuators A: Physical*, 2025, **386**, 116331.